Journal of Chromatography A, 657 (1993) 283–303
Elsevier Science Publishers B.V., Amsterdam

CHROM. 25 534

Hydrodynamic chromatography of polymers in packed columns

Gerrit Stegeman, Johan C. Kraak* and Hans Poppe

Laboratory for Analytical Chemistry, University of Amsterdam, Nieuwe Achtergracht 166, 1018 WV Amsterdam (Netherlands)

Robert Tijssen

Koninklijke/Shell-Laboratorium Amsterdam, Department AG/2, Badhuisweg 3, 1031 CM Amsterdam (Netherlands)

(First received June 14th, 1993; revised manuscript received August 30th, 1993)

ABSTRACT

Hydrodynamic chromatography (HDC) of linear random coil polymers in columns packed with 1.5-μm non-porous particles was investigated. For polymers with high molecular masses (10^4–10^7), the resolution appears to be almost independent of the eluent velocity. This allows for high-speed polymer separations with high efficiency. A model for the migration rate of polymers, based on the assumption that interstitial channels in a packed column can be represented by a bundle of capillary tubes, is compared with experimental elution data. The influence of polymer size and type, solvent goodness and mobile phase velocity on elution in HDC was investigated. Elution behaviour in packed columns appears to obey basically the simple migration theories developed for open tubes. The relative peak positions in the HDC trace depend slightly on the eluent velocity.

INTRODUCTION

Hydrodynamic chromatography (HDC) in packed or open-tubular columns is a technique able to separate macromolecules and particles according to size [1]. It has found application for the separation of a variety of samples in the (sub-)micrometre range such as polymer latices [2,3], flexible and rigid polymers [4–7], viruses [8], pollen [2,9], paper fibres [10,11], silica particles [9,12], proteins [4,13], DNAs [14] and liposomes [15].

DiMarzio and Guttman [16–18] were the first to give a theoretical explanation of the separation mechanism in HDC. They considered the flow of finite-sized dispersed particles through a capillary tube and concluded that the larger particles will have a higher average velocity than the smaller particles, because the particle centre cannot sample the lowest velocities on the streamlines near the wall, within a distance equal to the particle radius r_p (see Fig. 1). According to this simple exclusion model, the ratio of particle to tube radius, λ, determines to what extent the average particle velocity differs from the average solvent velocity. Despite its simplicity, this model is able to predict, at least qualitatively, the elution behaviour in capillary tubes and packed columns filled with non-porous particles.

In addition to steric exclusion, DiMarzio and Guttman also included hydrodynamic wall effects, which retard the particles with respect to the local undisturbed fluid velocity. In a refined theory by Brenner and Gaydos [19], these wall effects were described more accurately for flow in open tubes.

Small *et al.* [3,20] showed that the migration rate of polymer colloids in packed columns is

* Corresponding author.

0021-9673/93/$06.00

strongly influenced by colloidal forces between the colloids and the packing particles. Colloidal forces, including electrostatic and Van der Waals forces, influence the distribution of solute particles over the cross-section of a flow channel. Because of such forces, particles do not sample the accessible streamlines in a velocity profile with equal probability. Theoretical migration models which include colloidal forces were developed for flow in open tubes by Prieve and Hoysan [21], Silebi and McHugh [22] and Buffham [23]. These models were first applied to model the migration behaviour in packed columns by representing the interstitial channels as a bundle of circular tubes. Comparison with Small *et al.*'s data showed that trends in the elution behaviour can be predicted well but no exact fit is obtained unless model parameters are adjusted. A better agreement between these models and elution data was recently obtained in capillary HDC [24].

A further complication in the treatment of the separation mechanism in HDC is the effect of solvent flow-rate on the relative particle velocity (the ratio of the average particle velocity to the average solvent velocity). In capillary HDC the relative particle velocity was reported to increase with increasing eluent flow velocity by Noel *et al.* [9] and Silebi and DosRamos [24], the increase being more pronounced for larger particles. This phenomenon has been attributed to radial particle migration due to fluid inertia such as described by Segré and Silberberg [25]. This so-called "tubular pinch" effect was recently included in theoretical migration models for capillary tubes (together with colloidal forces, hydrodynamic wall effects and wall exclusion) by DosRamos and Silebi [26] and Ploehn [27]. Comparison of these detailed models with experimental results in open tubes showed that effects of flow-rate could be described satisfactorily. More generally, these models seem to provide a fairly comprehensive analysis of the separation process in which the variables affecting the migration of particles are well understood. In packed-column HDC the situation is much more complicated. It may be argued that flow-induced lateral migration can also be of importance here. Indeed, the flow-rate has been reported to influence the relative velocity of different types of samples, but the effects on the migration rate are opposite to those observed in open tubes [12,28,29]. Whether this can be (partly) attributed to lateral migration phenomena is still unclear at present. Alternative explanations in terms of shear orientation and shear deformation have been put forward.

In the study of the transport of flexible polymers in HDC, additional difficulties emerge. Size, shape and structure of the polymer are not known accurately, nor are their effects on polymer hydrodynamics. Besides, these parameters are subject to the influence of solvent, temperature, concentration and shear rate. Tijssen and co-workers [5,30] studied the migration rate of dissolved linear polystyrenes in open microcapillary tubes and compared this with refined theoretical models for the migration of rigid impermeable and permeable spheres. They found that these models are basically obeyed and only need small modifications to describe the transport of flexible polymers. In a similar study, the migration of polystyrenes in packed columns filled with 1.5–3.5-μm particles was investigated [12]. Experimental elution data were compared with modified capillary migration models in which flow-rate effects were not accounted for. Although a slight velocity dependence of the migration rate was observed for the ultra-high molecular masses, the agreement with the theoretical models was found to be good. This finding again demonstrated the usefulness of capillary migration models in modelling the migration behavior in packed columns.

In this work, the migration of flexible polymer in packed columns was further investigated. The effect of polymer size and coil segment density on the migration rate was studied in packed columns filled with 1.5-μm solid silica packing particles. Linear polystyrenes (PS), polyisoprenes (PIP), polybutadienes (PB) and poly(methyl methacrylate)s (PMMA) in both good and poor solvents were used as test samples. The observed elution behaviour was compared with predictions from a migration model that represents the interstitial channels in a packed column by open tubes. Flow-rate-dependent migration was studied and possible explanations are sug-

gested. Further, the separation power of the columns used was demonstrated by means of some high-resolution separations of polymers.

THEORY

Polymer size

In order to describe the factors that determine the dimensions of polymer molecules in solution, an adequate model for a polymer chain is required. A useful but inaccurate model for linear polymer molecules is the random-flight chain, which is a chain of segments connected by completely flexible joints [31,32]. The modelling of a polymer chain can be made more realistic by including short-range interactions that account for fixed bond angles and hindered internal rotation. This results in a so-called ideal or unperturbed chain which has a Gaussian segment density distribution. The molecular dimensions of such a chain, called the unperturbed dimensions, can be expressed conveniently in terms of the mean square radius of gyration $\langle r_G^2 \rangle_0$, according to

$$\langle r_G^2 \rangle_0 = \frac{\sigma l^2 n}{6} \quad (1)$$

where σ is a structural parameter or "conformation factor [32]", l is the segment length and n is the number of segments in the chain. The parameter σ (which is independent of n) describes the short-range interactions and has a value ≥ 1. When $\sigma = 1$, eqn. 1 represents the dimensions of a perfectly flexible random-flight chain.

On choosing different types of polymers, we can expect σ and l to vary considerably. As a result, the size and compactness of a chain are strongly dependent on the type of polymer. This will turn out to be an important aspect in this study.

In order to improve further the modelling of a polymer chain, long-range interactions need to be considered. For example, polymer segments occupy finite volumes and therefore exclude other segments from occupying the same space at the same time. This leads to a coil that is expanded compared with the unperturbed one. Further, the polymer–solvent interactions influence the coil dimensions by either expanding or contracting the coil. In a good solvent, the polymer–solvent interactions are thermodynamically favourable and solvent molecules will be imbibed, resulting in coil expansion. With a poor solvent, the solvent molecules will be squeezed out, contracting the polymer chain. The relative goodness of a solvent depends on the temperature and the nature of the polymer–solvent system.

In most circumstances, the long-range interactions will expand the polymer coil compared with the unperturbed dimensions. Occasionally, in very poor solvents, the polymer size can be smaller than the unperturbed dimensions. Including long-range interferences, the mean square radius of gyration of a linear macromolecule is written as

$$\langle r_G^2 \rangle = \alpha^2 \langle r_G^2 \rangle_0 \quad (2)$$

where α is the linear expansion factor, which in general depends on the number of bonds n. Only when $\alpha = 1$ do long-range expansion and contraction apparently cancel, and the polymer chain behaves like an unperturbed chain. This occurs under special conditions of solvent and temperature, known as θ-conditions. Under θ-conditions, the coil dimensions are predicted to be independent of the particular solvent used. This has indeed been found experimentally for non-polar polymers in non-polar solvents, but deviations occur in case of polar polymers and solvents [33].

From the modelling of polymer chains, the radius of gyration r_G $[= (\langle r_G^2 \rangle)^{1/2}]$ logically becomes the basic size parameter. In order to test the HDC migration models, reliable relationships between r_G and the molecular mass of polymers are required. Such relationships can be derived from measurements that directly yield r_G such as light-scattering or neutron-scattering measurements. These relationships are well documented for polymers in θ-solvents [34]. With good solvents however, such relationships are only known for a limited number of polymer–solvent combinations. Alternatively, approximate r_G–M relationships can be obtained indirectly from viscometric measurements. As vis-

cosity measurements are the most commonly used way to study polymer solutions, many data are available. For good solvents, the radius of gyration can be calculated according to the Flory–Fox and Ptitsyn–Eizner relationship [35,36]:

$$r_G = \frac{1}{\sqrt{6}} \left(\frac{KM^{1+a}}{\phi_0(1 - 2.63\beta + 2.86\beta^2)} \right)^{1/3} \quad \text{(cm)} \quad (3)$$

where the product KM^a is the polymer intrinsic viscosity, with K (in ml/g) and a being the Mark–Houwink constants, ϕ_0 is the Flory universal constant equal to $2.86 \cdot 10^{23}$ (mol^{-1}) and $\beta = (2a - 1)/3$.

As stated in the Introduction, the main mechanism behind separation in HDC is the exclusion of solutes from the wall. Therefore, the size parameter of interest is the one that determines exclusion from a wall. This radius will be called r_p throughout. With rigid spherical solutes, the term "size" is unambiguous, but for polymer chains with continuously changing shapes, the relationship between any kind of radius and the extent of exclusion is less clear. Van Kreveld and Van den Hoed [37] proposed that the actual radius of a linear random coil polymer determining exclusion is half of the mean maximum cross-section of the random coil. This so-called effective radius r_{eff} is related to r_G according to

$$r_{eff} = \frac{\sqrt{\pi}}{2} \cdot r_G \quad (4)$$

r_{eff} has been used successfully in modelling the migration of random coil polymers in SEC [37] and HDC [5,12]. Still, the problem of polymer size near a solid wall has not yet been fully solved, and size parameters other than r_{eff} have been proposed (see ref. 30 for a discussion).

Other frequently used size parameters are based on a hard sphere representation of a polymer coil [38]. The equivalent sphere representation naturally originates from the spherical shape of the time-averaged random coil conformations. Hard-sphere radii such as the hydrodynamic, the viscometric or the thermodynamic radius are apparent radii equal to the radii of a hard sphere of which a given physical property is the same as that of the polymer coil. As such equivalent sphere approaches are crude and limited models, the hard-sphere radii are not exactly related to r_G. In this study, a polymer hard-sphere radius used in a general sense will be termed r_s. The hydrodynamic radius is denoted r_h.

Flow permeability of polymers

An important aspect in describing the hydrodynamic behaviour of polymers is the flow permeability of the chain. In this regard, two limits may be considered: the free-draining and the non-draining limit. In the free-draining limit, all chain segments experience the flow as if it were undisturbed by other segments. In other words, the chain is seen as an assembly of independent hydrodynamic units. In the non-free-draining limit, the solvent in the interior of the chain domain is immobilized with respect to the chain and the polymer behaves as hydrodynamically impermeable to the flow. A transition from free-draining to non-free-draining is predicted with increasing n, as chain segments in the centre are then becoming increasingly shielded.

Viscometric measurements proved that, except for a very low degree of polymerization, polymer chains behave practically as non-free-draining [32]. The same conclusions can be drawn from theoretical calculations, which showed that indeed the solvent in the interior of a polymer coil is almost stationary with respect to the coil [39]. On the other hand, the same calculations also indicated that the flow permeability of the chain increased substantially on going from the centre to the outside of the polymer.

Hence the chain as a whole can be considered as an almost impermeable hydrodynamic body, although microscopically the picture is more complicated.

Migration behaviour of polymers in packed columns

Deriving theoretical models for the migration of polymers in flowing media is complicated. Adequate modelling is actually restricted to simple flow geometries such as circular tubes. Attempts to tackle more difficult flow systems for this reason necessarily fall back on simplified

channel geometries. In this study in which polymer migration in packed columns is treated, the interstitial channels are represented by a parallel array of capillaries of equal size. Following earlier work in this field, we take as the equivalent capillary radius the hydraulic radius R_0, which is the radius of a capillary tube with equal volume-to-surface ratio as the packed bed [1,12,21]:

$$R_0 = \frac{d_p}{3} \cdot \frac{\epsilon}{1-\epsilon} \quad (5)$$

where d_p is the diameter of the packing particles and ϵ is the column porosity, which is the ratio of the interstitial liquid volume V_0 to the total column volume V_c. The simplifying assumptions on flow channel geometry allow for the use of capillary migration models. Consequently, in this section we shall focus further on the migration of polymers in open tubes.

In a tube of radius R an expression for the mean axial velocity $\langle v_p \rangle$ of a spherical particle or polymer with radius r_p is [19]

$$\langle v_p \rangle = \frac{\int_0^{R-r_p} v_p(r)\, e^{-E(r)} r\, dr}{\int_0^{R-r_p} e^{-E(r)} r\, dr} \quad (6)$$

where $v_p(r)$ is the local axial velocity of the particle and $E(r)$ is the dimensionless total potential experienced by a particle due to interactions with the capillary wall. The upper limit of integration $R - r_p$ accounts for the exclusion of the solute centre from the wall region.

In general, a non-zero value of $E(r)$ will cause the accessible radial positions in the tube to be sampled with unequal probability, leading to a radial concentration profile. $E(r)$ can contain colloidal interactions but may also include hydrodynamic forces in the form of a hydrodynamic "potential". Since in our study we focus on the migration behaviour of polymers dissolved in organic solvents, we assume that colloidal forces are absent. In capillary HDC it was shown that hydrodynamic forces cannot be omitted. A substantial influence, expressed in a flow-rate-dependent migration rate, was observed, even for solutes as small as dissolved polymers [30]. Whether hydrodynamic forces can also be significant in packed columns is not certain. Including hydrodynamic forces in migration models is very complicated. Only for flow in channels of fairly simple geometry (*i.e.*, flow in open tubes or between parallel plates), semi-empirical models have been developed [26,27,30]. Such theories, however, certainly cannot be applied directly to packed columns. In this study we shall not attempt to formulate a theory for hydrodynamic forces in packed columns. Rather, we shall neglect these forces for the moment and treat them only qualitatively in a subsequent section on flow-rate-dependent migration behaviour.

Neglecting lateral forces on the polymer molecules, we assume that all radial positions are sampled with equal probability except those in the exclusion layer (see Fig. 1). The local axial particle velocity $v_p(r)$ in a cylindrical tube can then be expressed as

$$v_p(r) = 2\langle v_m \rangle \left(1 - \frac{r^2}{R^2}\right) - v_s(r) \quad (7)$$

where $\langle v_m \rangle$ is the average velocity of the mobile phase and $v_s(r)$ is the slip velocity of the particle. The slip velocity describes the extent to which the centre of mass of a neutrally buoyant particle lags the local (unperturbed) eluent velocity. For homogeneous solid spheres, it has been found that the slip velocity depends on radial position r and on the ratio of the particle to tube radius. According to Brenner [40] and Goldman *et al.* [41], the slip velocity can be expressed as

$$v_s(r) = \gamma(r)\langle v_m \rangle \left(\frac{r_p}{R}\right)^2 = \gamma(r)\langle v_m \rangle \lambda^2 \quad (8)$$

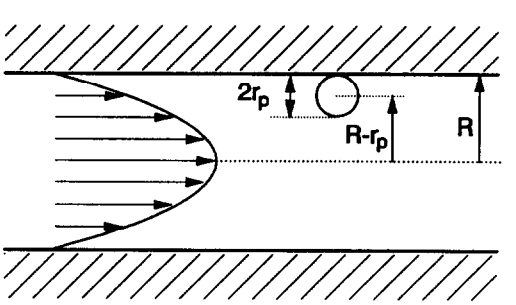

Fig. 1. Transport of a spherical particle immersed in Poiseuille flow through a cylindrical capillary.

where $\gamma(r)$ is the wall-effect parameter and λ is defined as the ratio r_p/R. $\gamma(r)$ is a function of the radial position and λ. In the centre of the tube $\gamma(r) = 4/3$.

In a pioneering effort to derive an expression for the slip velocity of free-draining polymers in Poiseuille flow through an open tube, DiMarzio and Guttman [17] represented the polymer molecule by a rigid sphere that is permeable to the solvent. They arrived at the following expression for the slip velocity:

$$v_s(r) = \gamma \langle v_m \rangle \left(\frac{r_G}{R}\right)^2 \tag{9}$$

In the approach of DiMarzio and Guttman, $\gamma = 4/3$ at every radial position and for every value of λ. Brenner and Gaydos argued that this is not entirely correct, because in this expression the hydrodynamic retardation of a sphere in the direct neighbourhood of the wall is not properly accounted for [17,19]. Strictly, eqn. 9 is not valid over the whole cross-section of the tube but only represents the slip at the axis. Keeping this in mind, there is a remarkable similarity between eqn. 9 and the expression obtained for the slip of a solid sphere in the centre of a tube (see eqn. 8). The difference between the permeable-sphere and the solid-sphere approach is apparently reflected in different radii in the expression for $v_s(r)$. For solid spheres the slip velocity is related to r_p whereas for permeable spheres a dependence on r_G is found (note that for both permeable and solid rigid spheres with a homogeneous mass distribution, $r_G = \sqrt{3/5} \cdot r_p$). Whether this means that the entire solid-sphere theory can be carried over to permeable spheres by simply replacing the solid sphere radius by r_G is not certain.

After substitution of expressions for $v_s(r)$ in eqn. 7 and carrying out the integrations in eqn. 6, a general expression for the mean particle velocity in laminar tube flow is obtained:

$$\langle v_p \rangle = \langle v_m \rangle (1 + 2\lambda - C\lambda^2) \tag{10}$$

or, in terms of a relative migration parameter τ [5],

$$\tau = \frac{\langle v_m \rangle}{\langle v_p \rangle} = (1 + 2\lambda - C\lambda^2)^{-1} \tag{11}$$

According to the basic separation mechanism (see Fig. 1 and eqn. 6), λ should be based on the size of a polymer or particle near the wall. In both the DiMarzio–Guttman and the Brenner–Gaydos model, where rigid spheres are considered, the definition of r_p (and thus λ) is enequivocal. The C value varies on choosing different expressions for v_s. In the solid-sphere model by Brenner and Gaydos, both v_s and λ are functions of r_p. The C value in this model becomes [19]

$$C_{BG} = 1 + \frac{\frac{4}{3} + 2.56}{(1-\lambda)^2} \tag{12}$$

In the permeable sphere model by DiMarzio and Guttman where the slip velocity is based on r_G rather than on the particle size near the wall, the C value is [17]

$$C_{DG} = 1 + \frac{4}{3}\left(\frac{r_G}{r_p}\right)^2 \tag{13}$$

A major reason why modelling the transport of polymers is far more complicated than that of rigid spherical particles is that size and shape of the polymer are not well defined. Even when treating polymer molecules as rigid spheres, the problem of attributing the correct size to a polymer coil remains. The polymer size of primary interest in HDC is the radius near a solid wall, r_p, or better, the distance to which the mass centre of the polymer molecule can approach the wall. This size cannot be determined accurately by experimental methods.

Further, an adequate description of the hydrodynamic structure of polymer chains is very difficult. As was discussed already, the free-draining concept of polymer chains is inconsistent with experimental results, making the permeable sphere model an unrealistic picture of a real polymer coil. The nearly impermeable interior of a polymer chain is likely to be approximated better by a solid sphere, but whether the homogeneous solid sphere is able to provide a good representation of the entire polymer coil is questionable. Yet we are left with these simplified models because more sophisticated models of polymer chains are not easily

accounted for in the analysis of transport phenomena.

Tijssen *et al.* [5] compared the Brenner–Gaydos and DiMarzio–Guttman models with the retention behaviour of dissolved polystyrenes in microcapillary tubes. They modified both models in several ways, in order to apply them to random coils polymers. For polystyrenes in a good solvent, they found that the migration behaviour agreed best with a modified DiMarzio–Guttman model, in which the polymer radius r_{eff} is substituted for r_p. In a θ-solvent, experimental data were predicted well by the same model, provided $r_p = r_G$ was chosen. Recent measurements show that also for good solvents, experimental results are best fitted when r_G is taken as the polymer radius [30].

Surprisingly, the more refined Brenner–Gaydos model, and modified versions of it, did not well fit the experimental results. All theoretical C values were obviously too high to give a good match between theory and experiment. In the modifications of the Brenner–Gaydos model, Tijssen *et al.* replaced the solid-sphere radius in the expressions for the slip velocity by r_G. As was shown by DiMarzio and Guttman [17] for solutes in the centre of the tube, this corresponds to changing the particle structure from impermeable to permeable. In view of the almost impermeable character of the polymer coil, a physically more feasible approach would be to apply the original solid-sphere model and rather define a suitable hard-sphere radius for a polymer chain. For random coil polymers, the hard-sphere radius in the expressions for the slip velocity need not necessarily be the same as the effective radius near the wall. This can be expressed in a modification of C_{BG}:

$$C_{BG} = 1 + \frac{\frac{4}{3} + 2.56}{\left(1 - \frac{r_s}{R}\right)^2} \cdot \left(\frac{r_s}{r_p}\right)^2 \qquad (14)$$

where r_s is the radius of an (equivalent) solid sphere. The term r_s/r_p accounts for the different characteristic radii upon which λ and $v_s(r)$ are based. A similar term appeared in the DiMarzio–Guttman model (eqn. 13). Obviously, eqn. 14 reduces to eqn. 12 when homogeneous solid spheres are considered, since then r_s is equal to r_p.

A suitable candidate for the hard-sphere radius of a polymer may be the hydrodynamic radius r_h. For different types of linear random coil polymers in both good and poor solvents, $r_h = 0.66$–$0.80\ r_G$ [38,42]. The C value obtained when substituting r_h for the hard-sphere radius r_s in eqn. 14 is lower than in Tijssen *et al.*'s modifications of the Brenner–Gaydos model. As the C values in the former modifications (and in the original model) were too high to fit experimental migration data in capillary HDC well [5], a better agreement is expected with the present approach. Our modification of the Brenner–Gaydos model yields theoretical calibration graphs close to those from the modified DiMarzio–Guttman permeable sphere model, which so far was most successful in describing the migration behaviour of polymers in open tubes.

The modified DiMarzio–Guttman model was also found to predict surprisingly well the retention behaviour in packed columns [12]. On replacing the tube radius R by the hydraulic radius R_0, the DiMarzio–Guttman model with $r_p = r_{eff}$ accurately matched the retention data for polystyrenes in tetrahydrofuran. This finding strongly encouraged further research in this area. The DiMarzio–Guttman model will be the basis for the present investigation of trends in the migration behaviour induced by polymer structure and solvent nature.

Effect of flow-rate on the migration of polymers

In the migration models discussed so far, it was assumed that all positions in a flow channel are sampled with equal probability, except those in the inaccessible exclusion layer near the wall. However, many experimental observations and theoretical considerations indicate that phenomena exist that can cause non-random sampling. In this section a survey is given of such phenomena, but only those where the distribution of polymers in the flow channel is dependent on eluent velocity will be treated (electrostatic forces will thus be neglected). A more extensive review of anomalous effects in wall-bounded

sheared flows of polymer solutions and particles can be found in refs. 43 and 44.

Stress-induced diffusion (SID). In simple laminar shear flow in a tube, high stress regions near the wall and low stress regions near the centre can be distinguished. In the high-stress regions, polymer molecules can be elongated and oriented. As a consequence, polymers near the wall have a lower entropy than polymers situated near the tube axis. This entropy gradient causes a cross-streamline migration away from the wall [44–47]. This leads to a concentration build-up in the centre of the tube and a depleted layer near the wall. Cross-streamline migration due to SID is strongly favoured by higher flow-rates, smaller tube diameters and higher molecular masses.

When a packed column with non-porous particles is considered, SID will lead to migration of polymers away from the wall, causing τ to decrease with increasing velocity. On the other hand, when porous particles are employed, it has been argued that SID is likely to cause a concentration build-up in the pores. For this reason, SID has been put forward as an explanation for observed flow-rate-dependent migration behaviour in size-exclusion chromatography (SEC) [48].

In packed-column HDC, where the velocity gradients can be sufficiently high to cause deformation of larger polymer molecules [6,8], the occurrence of SID is not unlikely. Unfortunately, a quantitative treatment of SID is difficult, especially when complicated flows such as those in packed columns are concerned. Further, the development of a lateral concentration profile in the inter-particle channels is counteracted by stream splitting around the packing particles. At present it is not clear if stream splitting can fully nullify the effect of SID under experimental conditions in HDC.

SID has been put forward as a likely cause of flow enhancement, which has been observed for flow of polymer solutions in open tubes and in various porous media including packed columns [44]. Flow enhancement means that experimentally measured flow-rates at a given stress level are much higher than predicted from cone-and-plate viscometer measurements.

Polymer deformation. When polymers are deformed in sheared flow, this may not only cause SID, but a deformation-induced change in polymer size and shape itself can also influence the migration rate. If a polymer becomes elongated the size transverse to the direction of flow decreases and thus λ decreases. When only this effect of size is considered, while further assuming random sampling of accessible positions in the flow channel, the migration behaviour will be flow-rate dependent [6,8]. At higher velocities, polymers elute at larger τ and thus mimic lower molecular masses. This flow effect is enhanced by increasing flow velocity, increasing molecular mass or decreasing flow channel dimensions.

Molecular stretching occurs only when the flow is sufficiently "strong" or, in other words, when elongating forces are no longer offset by chain relaxation [8]. A measure of the extent of deformation is the Deborah number, *De*, which is the product of the relaxation time and the elongation rate. At $De > 0.1$ the polymer is stretched to such an extent that flow-rate-dependent migration may be observed in HDC. Under the usual chromatographic conditions in HDC, *De* may well exceed 0.1 for large, flexible molecules. Experiment results have indeed shown that elution in HDC begins to shift towards a smaller apparent solute size at the onset of deformation [8,49].

Hoagland and Prud'homme [6,8] observed that the elution volume of flexible and stiff macromolecules in packed column HDC depends on the eluent velocity. They concluded that this might well be explained by shear-induced orientation and deformation. Good agreement was found between calculated cross-sectional diameters of deformed random coil polymers (modelled as deformed Rouse chains) and the dimensions calculated from HDC elution data for hydrolysed polyacrylamides. Also, for stiff xanthan molecules, the measured effect of flow-rate on τ could be predicted reasonably well using the theory of shear orientation of dumbbell type macromolecules.

The deformation-induced change in polymer size and SID affect the elution of polymers in the opposite direction. The size effect produces higher τ values with increasing eluent velocity, whereas SID does the contrary. One might argue

that they are somehow coupled to cause an overall effect on τ, which depends on the degree of deformation. Measurements of pressure drop *versus* velocity for dilute polymer solutions in porous media may point in this direction, as stated by Cohen [44]. It was found that the pressure drop was lower than expected if the flow velocity was below the point of significant polymer deformation ($De \approx 0.1$). This flow enhancement was suggested to be caused by cross-streamline migration (owing to SID). For much higher flow velocities, beyond the point of polymer deformation, flow retardation (*i.e.*, reduction) was observed, which may be indicative of shear deformation.

Inertial radial migration. A sphere under viscous flow in a tube may undergo a radial force resulting from fluid inertia. This makes particles migrate across streamlines into an annular region around the equilibrium position at about 0.6 tube radius distance from the tube axis. The influence of inertial forces becomes more pronounced with increasing flow, increasing particle diameter and decreasing radius of the tube [30].

DosRamos and Silebi [26], Ploehn [27] and Tijssen and Bos [30] incorporated radial migration by fluid inertia in residence theories for capillary HDC. Comparison with experimental results showed that this could indeed explain observed flow-rate-dependent migration. The findings in open tubes suggest that inertial effects may also affect the elution of polymers in packed columns. However, in packed columns their influence is probably less pronounced. This is in the first place because the achievement of steady-state concentration profile is prevented by the randomizing effect of stream splitting around packing particles. For flow in open tubes it was pointed out by Ploehn that a steady-state concentration profile, under normal operating conditions, requires tube lengths that are several orders of magnitude larger than the tube diameter. When the same argument applies to packed columns, a concentration build-up by inertial lateral migration will be largely undone by stream splitting and a steady-state concentration profile will certainly not be effected. Further, the flow velocities commonly employed in packed columns are lower than in capillary HDC. The influence of inertial forces on the distribution of solutes in the flow channel will therefore not be very large even if a steady state were attained in packed columns. In open tubes the inertia induced effect of flow velocity on τ can be considered insignificant when the dimensionless group $Pe\ \lambda^2 < 1$ [30], where Pe is the Péclet number ($Pe = 2\langle v_m \rangle R/D_m$, where D_m is the molecular diffusion coefficient). A comparable criterion derived by Silebi and McHugh [22] states that inertial forces are negligible unless the product of the particle Reynolds number, Re_p, and Pe exceeds 3. Under chromatographic conditions, these criteria are mostly not fulfilled. Inertial lateral migration may become significant only for the largest permitted solute sizes.

Hydrodynamically induced diffusion (HID). Several investigators have used a kinetic theory approach to describe the diffusion of bead-spring-type macromolecules in inhomogeneous flows. Aubert and Tirrell [50,51] found theoretically that such molecules with volumeless beads will migrate in the concave-side direction across curvilinear streamlines, because of the inability of the molecules to align with the flow. In this theory, lateral drift in rectilinear flow was not predicted. However, when including finite bead volume and hydrodynamic interactions, macromolecular migration is predicted across parallel streamlines in Poiseuille flow also [52–54]. The approach for parallel streamlines leads to polymer migration away from the wall, in agreement with the entropic theory of SID.

Radial migration of polymers in the concave-side direction in curved flows was confirmed experimentally in circular couette flow [55]. It was speculated that the curved streamlines in packed-column flow could also cause polymer migration towards the surface of the packing particles. Theory predicts that such migration would be enhanced by higher eluent velocities and higher molecular masses. In SEC this cross-streamline migration would tend to increase the polymer concentration in the pores with increasing velocity and this effect is expected to be more pronounced for higher molecular masses. Elution data supporting this mechanism have been reported [56].

Multi-path effect. Another mechanism able to increase the polymer concentration near the wall is the multi-path effect, described by Giddings [57]. Large molecules are forced against the wall when flow channels split around packing particles and streamlines graze within a distance r_p from the packing particles. This will lead to polymer concentrations higher than the equilibrium values near the surface. Further, polymers may become trapped in apertures between particles. Giddings speculated that escape from wall regions and apertures would depend on the polymer diffusion coefficient. He assumed that polymer retardation by the multi-path effect increases with increasing molecular mass and increasing flow-rate. The multi-path effect has not yet been proved experimentally, nor has it been expressed in theoretical models.

EXPERIMENTAL

Materials and chemicals

The solvents used were analytical-reagent grade tetrahydrofuran (THF), 1,4-dioxane, toluene, methanol and ethyl methyl ketone from Merck (Darmstadt, Germany) and acetonitrile from Janssen (Geel, Belgium). Before use the solvents were filtered through a 0.1-μm inorganic membrane filter (Anodisc 47; Anotec, Banbury, UK). Empty stainless-steel columns with dimensions 150 × 4.6 mm I.D. were obtained from Chrompack (Middelburg, Netherlands). The non-porous packing particles were a gift from Professor K.K. Unger (Johannes Gutenberg Universität, Mainz, Germany). Polystyrene (PS) standards of narrow molecular mass distribution were obtained from Merck, Machery–Nagel (Düren, Germany) and Toyo Soda (Tokyo, Japan). Polyisoprene (PIP), polybutadiene (PB) and poly(methyl methacrylate) (PMMA) standards were purchased from Polymer Laboratories (Church Stretton, Shropshire, UK). The most relevant data of these polymer fractions are summarized in Table I.

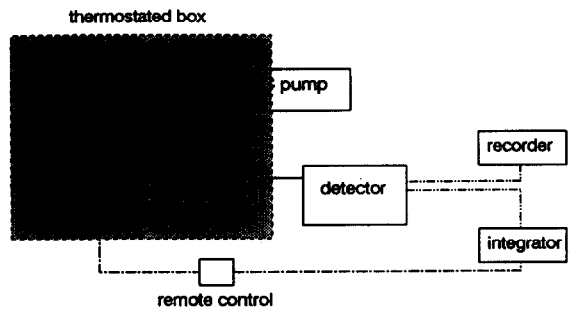

Fig. 2. Schematic representation of the experimental set-up for packed-column HDC.

Apparatus

In Fig. 2 the experimental set-up for packed-column HDC is shown schematically. Several parts of the equipment were placed in a laboratory-built air-thermostated box with polycarbo-

TABLE I

CHARACTERISTIC DATA FOR THE POLYMER STANDARDS

Polymer	Isomer composition[a] (microstructure)	M_w range ($\times 10^{-3}$)	Range of M_w/M_n ceiling values[a]	Supplier
PS		0.58–1260	1.04–1.18	Merck
PS		336–7700	1.03–1.2	Macherey-Nagel
PS		43.9 and 775	1.01	Toyo Soda
PB	45% *cis*, 49% *trans*, 6% vinyl	0.90–950	1.02–1.08	Polymer Laboratories
PIP	87% *cis*, 9% *trans*, 4% vinyl	1.35–3300	1.02–1.07	Polymer Laboratories
PMMA		2.40–1400	1.04–1.09	Polymer Laboratories

[a] Manufacturers' data.

nate walls. The temperature inside the box was registered by two calibrated electronic thermometers (Amarell, Kreuzwertheim, Germany). The HPLC pump (Spectroflow 400; ABI, Ramsey, NJ, USA) was partially thermostated, the control panel remaining outside the box. The pneumatically driven injection valve had a 1-μl internal sample loop (Ci4W; VICI, Houston, TX, USA). High-speed switching of this valve was allowed by a HSSA speed-up kit (VICI). The detector was either a variable-wavelength UV detector (Spectroflow 757; ABI) operated at 210 nm or an evaporative light-scattering detector (ELSD IIA; Varex, Burtonsville, MD, USA).

Both detectors were slightly modified to minimize their contribution to peak broadening and reduce their hold-up volume. The conventional 8-μl UV detection cell was replaced with a capillary flow cell (ABI). In this arrangement a small length of a 100 μm I.D. fused-silica capillary served as a detection cell, after removing the polymer coating. The fused-silica capillary was directly coupled to the column outlet, the length of tubing between column and detection window being 15 cm. The ELSD was connected to the column by a 75 μm I.D. fused-silica tube of length 20 cm. This capillary was directly connected to the nebulizer, after removing the original stainless-steel connection tubing. This modification reduced the equivalent liquid dead volume of the ELSD to less than 3 μl under all measuring conditions.

The retention times were measured using an integrator (Model 3390A; Hewlett-Packard, Avondale, PA, USA). Integrator runs and chromatographic runs were started simultaneously by means of a laboratory-built remote control. Chromatograms were recorded on a potentiometric recorder (Kompensograph 3; Siemens, Karlsruhe, Germany).

Column packing and characterization

Three columns were packed with non-porous silica particles according to a previously described slurry-packing procedure [12]. After evaluation of plate heights and peak shapes, one column was chosen to study the migration behaviour of polymers. Important properties of this column are summarized in Table II. The size and

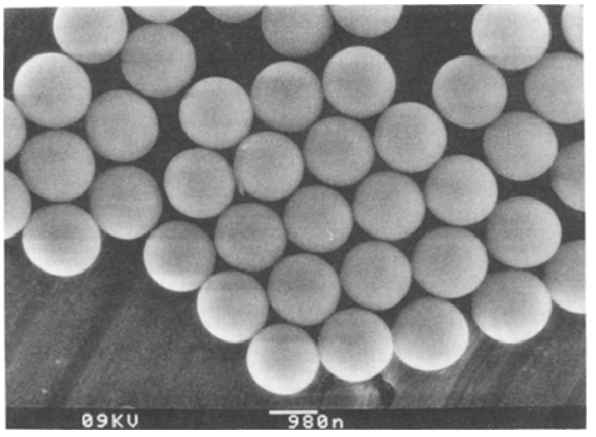

Fig. 3. Electron micrograph of 1.50-μm non-porous silica packing particles.

size distribution of the packing particles were determined using a scanning electron microscope (DS 130; ISI, Tokyo, Japan). The electron micrograph in Fig. 3 shows the very narrow size distribution of the particles. The reported particle diameter in Table II is the number-average diameter, measured for 50 particles. The mass difference between an ethanol-filled and a water-filled packed column was used to calculate V_0. This experiment was carried out in a thermostated box. A density meter (DMA 10; Paar, Graz, Austria) was used to determine accurately the density of ethanol. After emptying the column, the weighing procedure was repeated to find the total (empty) column volume. The column resistance parameter φ was calculated according to

TABLE II

COLUMN DATA

Parameter	Value
d_p (μm)	1.50 ± 0.03[b]
V_0 (μl)	1005
V_c (μl)	2550
ϵ	0.394
R_0 (μm)[a]	0.325
φ	410

[a] According to eqn. 5.
[b] Error indicates standard deviation.

$$\varphi = \frac{\Delta P d_p^2}{\langle v_m \rangle \eta L} \quad (15)$$

where ΔP is the pressure drop, η is the eluent viscosity and L is the column length.

Preparation of polymer solutions

Polymer concentrations was chosen to be as low as possible to prevent viscosity effects and to preclude effects of concentration on polymer size. When using the ELSD, the concentrations were typically around 0.05 mg/ml for the higher molecular masses and around 0.1 mg/ml for the lower molecular masses. With UV detection the concentrations were twice as high.

After adding the solvent, the polymers were allowed to swell and dissolve slowly for at least 16 h in a dark room. During this period, the polymers in good solvents were kept at room temperature, while the polymers in poor solvents were stored 5°C above the θ-temperature. Next, the solutions were homogenized by swirling slowly. Finally, they were stored at the column temperature until use. In order to prevent oxidation, PIP and PB solutions were stored under nitrogen. No solutions were used later than 2 days after preparation.

Determination of Mark–Houwink constants

For PB, PIP and PMMA, Mark–Houwink constants were determined in THF using SEC–viscometry. The SEC column used was a PLGEL Mixed D column from Polymer Laboratories. This viscosity detector was a capillary viscometer (H502; Viscotek, Porter, TX, USA). The Mark–Houwink constants were determined for molecular masses higher than 10^4.

Chromatographic measurements

All chromatographic measurements were performed at room temperature (23 ± 2°C), unless stated otherwise. For the measurements requiring careful temperature control, such as those for θ-solvents, the temperature variation was less than ±0.1°C from the desired value.

The polymer migration rate is expressed in terms of the dimensionless quantity τ; τ values are calculated as the ratio of the retention time of a polymer to that of a small unaccelerated "marker" molecule. Toluene was used as a marker when using UV detection. For the ELSD a less volatile marker was required and PS 580 was selected. All measurements using the latter marker were corrected for the small difference in migration rate between PS 580 and toluene ($\tau_{PS\,580} = 0.9963$). This correction factor, determined for THF, was assumed to be the same in other solvents. If the polymer of interest and the marker could be baseline resolved, they were injected simultaneously, otherwise they were injected with a time interval of 2 min in between. The measured τ values, presented as points in the figures, are averages of at least three measurements.

RESULTS AND DISCUSSION

Column efficiency

In previous work, dispersion characteristics of the columns used were studied [58]. As a major result, it appeared that plate heights were virtually independent of M_w and of eluent velocity for reduced velocities over 5. For molecular masses that are of actual interest ($M_w > 10^4$), this means that plate height is virtually constant in the usual range of eluent velocities. Moreover, dispersion appeared to be very low for these polymers. Measured plate heights were found to be lower than 2.5 μm in the selected range of eluent velocities. For the three columns tested, the minimum plate heights were 2.0, 2.0 and 1.9 μm. This shows that efficient columns can be packed reproducibly with very small non-porous particles.

The flat plate height–velocity curves indicate that a high separation speed is possible without a decrease in resolution. This is in contrast to polymer separation techniques such as SEC and normal-mode field-flow fractionation, where the theoretical plate heights increase rapidly with increasing velocity [59,60]. In practice however, the analysis speed is limited by the pressure drop across the column. This limitation is not too severe for the 1.5-μm particles, because of the

low flow resistance parameter φ (see Table II). Other limitations such as shear degradation of polymers at high eluent velocities might be more restrictive in HDC [60].

An illustration of a rapid separation of PS is displayed in Fig. 4. A baseline separation in 90 s is obtained between polymers differing a factor of two in molecular mass. At this high eluent velocity, the peak shape becomes slightly tailing. We believe this to result from the higher viscosity of the sample solution. Peak tailing could be diminished by choosing either a lower polymer concentration or a lower eluent velocity.

Other examples of high-resolution separations of PB and PIP, using the ELSD, are given in Figs. 5 and 6. Owing to the high sensitivity of the ELSD, polymer concentrations could be lower than 0.1 mg/ml. The high resolving power of packed-column HDC is clearly shown by the separation of PIP fractions in Fig. 6, where the highest selectivity and thus the highest resolution, normalized on molecular mass ratio, is obtained for molecular masses between $1 \cdot 10^5$ and $5 \cdot 10^6$. Although the molecular size of the polymer fraction eluted secondly is only 1.5 times the size of fraction number 3, a very high resolution is obtained. For smaller polymers, the resolution for a given fractional difference in molecular mass is much lower. In the high-selectivity part of the chromatogram, peak widths are probably also determined by the polydispersity of the polymer fractions. The resolution might have been higher if monodisperse fractions had been used.

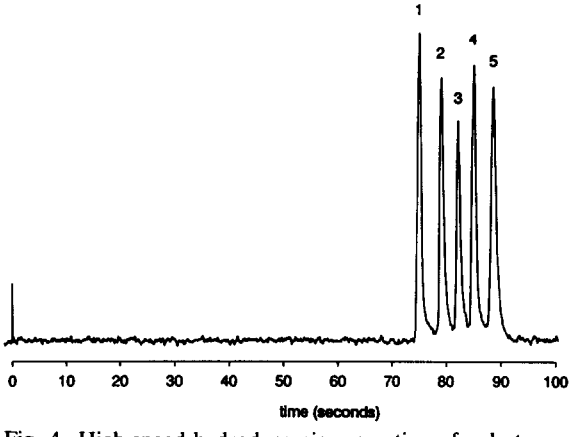

Fig. 4. High-speed hydrodynamic separation of polystyrenes dissolved in THF. Column, 150 × 4.6 mm I.D.; packing, 1.50-μm non-porous silica particles; pressure drop, 200 bar; detection, UV. Solutes: (1) PS 775 000, (2) PS 336 000, (3) PS 127 000, (4) PS 43 900 and (5) toluene, dissolved in THF (0.2 mg/ml each).

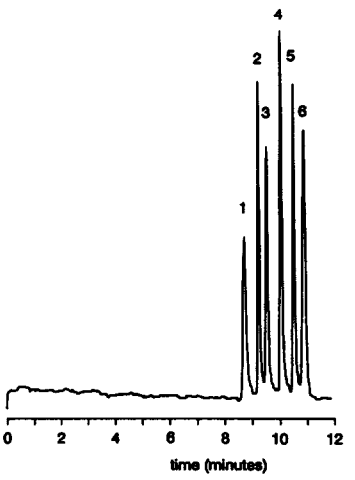

Fig. 5. Hydrodynamic separation of polybutadienes dissolved in THF. Column as in Fig. 4; pressure drop, 28 bar; detection, ELSD. Solutes: (1) PB 950 000, (2) PB 500 000, (3) PB 330 000, (4) PB 120 000, (5) PB 31 400 and (6) PB 3000 (0.06–0.10 mg/ml each).

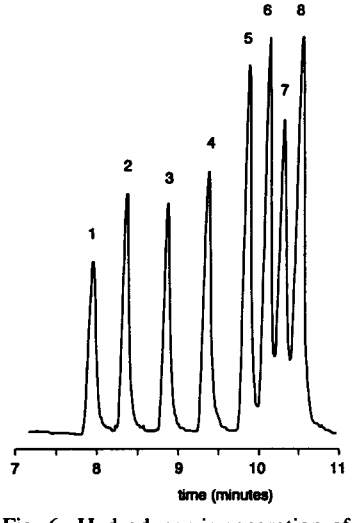

Fig. 6. Hydrodynamic separation of polyisoprenes dissolved in THF. Column as in Fig. 4; pressure drop, 29 bar; detection, ELSD. Solutes: (1) PIP 3 300 000, (2) PIP 1 200 000, (3) PIP 590 000, (4) PIP 295 000, (5) PIP 115 000, (6) PIP 60 000, (7) PIP 27 000 and (8) PIP 8000 (0.06–0.10 mg/ml each).

Effect of eluent velocity on τ

In the derivation of simple migration models, we excluded possible effects of the eluent velocity on τ. This was mainly because effects of flow velocity are not easily described in simple expressions, especially not when the flow in packed columns is considered. Moreover, a number of phenomena can be responsible for velocity-dependent τ-values. At present it is then unclear to what extent the mentioned flow effects influence τ. It is not even clear in what direction τ is predicted to alter when the eluent velocity is changed. Polymer deformation, HID and the multi-path effect predict that τ increases with increasing velocity, whereas SID and inertial migration predict the opposite. Experimental results in support of both trends have been reported. Measurements in packed-column HDC either suggest velocity-independent τ values [22] or point at an increase in τ with increasing velocity. The latter was only observed for high velocities and high molecular masses [8,12].

In order to elucidate possible effects of eluent velocity on τ further, the migration rate of polymers was studied at different eluent velocities. Velocities were chosen in a chromatographically useful range from 0.06 to 0.5 mm/s. The outcome of these experiments for PS in THF, and modified migration models, are shown in Fig. 7. The theoretical lines in this figure are drawn according to eqn. 11, using C_{DG} from eqn. 13 and C_{BG} from eqn. 14.

Starting at the lowest eluent velocity we observe a decrease in τ with increasing velocity until an apparent minimum value is reached. A further increase in eluent velocity then decreases τ. The velocity-dependent shifts in τ are largest for the highest molecular masses. In addition, the velocity at which a minimum τ value is achieved decreases with increasing molecular mass. For molecular masses below 10^6, the turnaround point for τ was not yet reached at the highest velocity.

Similar trends in the elution behaviour were also found for the other polymer types (PB, PIP and PMMA). In both good an poor solvents, the same velocity dependence of τ was observed. For a given molecular mass, the shifts in τ were approximately equal, irrespective of the polymer–solvent combination used. Apparently, the influence of polymer type and solvent on coil dimensions and coil structure is not large enough to significantly affect the observed shifts.

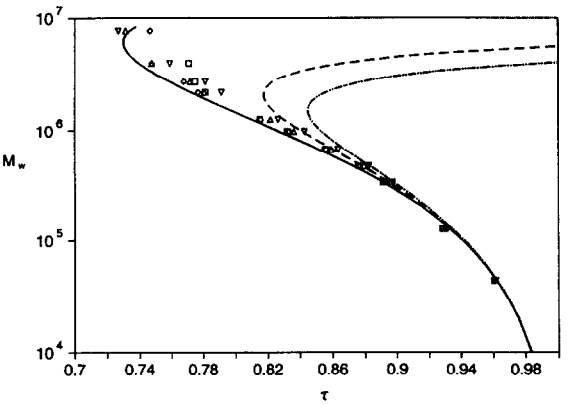

Fig. 7. Theoretical calibration graphs and experimental migration data for polystyrenes in THF. Column as in Fig. 4. Theoretical graphs: modified DiMarzio–Guttman model according to eqn. 13 with $r_p = r_{eff}$ (——), modified Brenner–Gaydos model according to eqn. 14 with $r_s = r_h = 0.7r_G$ and $r_p = r_{eff}$ (– – –) and modified Brenner–Gaydos model according to eqn. 14 with $r_s = r_h = 0.8r_G$ and $r_p = r_{eff}$ (– · · – · · –). The relationship between r_G and M_w is taken from ref. 5. Eluent velocity: (▽) 0.063, (△) 0.10, (◇) 0.22 and (□) 0.47 mm/s.

The explanation for the observed velocity-dependent migration behaviour is not straightforward. In previous work it was already found that at higher velocities τ increases with increasing $\langle v_m \rangle$. These observations could be reasonably well explained by considering the decline in transverse polymer size due to shear deformation. The opposite effect of eluent velocity on τ at low velocities has not been reported before. Possibly this effect is connected with the flow enhancement, observed in the flow of polymer solutions in porous media [44]. It has been suggested that flow enhancement may be caused by SID of polymers from the wall. Flow phenomena in packed columns are so poorly described, however, that other explanations are just as acceptable. A combination of two or more phenomena seems plausible.

In both the DiMarzio–Guttman and Brenner–Gaydos models, τ values are independent of eluent velocity, in contrast to our experimental results. In order to decide which of the models is

best we in fact require velocity-independent migration data. One may speculate that such data can be obtained only at much lower flow-rates than currently employed. Additional measurements are required to clarify this.

From a practical point of view, very low eluent velocities are not desired in HDC, because the analysis speed should be sufficiently high. We therefore have to accept a working range of eluent velocities in which τ is slightly dependent on $\langle v_m \rangle$. In the chromatographically useful range of higher velocities, the elution behaviour of polystyrenes can be described well by the DiMarzio–Guttman model.

From Fig. 7, it appears that at $\langle v_m \rangle = 0.22$ mm/s, minimum τ values are obtained for PS in THF over a wide range of molecular masses. The same was also found for other polymer–solvent combinations. In the next part, this velocity was selected to study in more detail the migration behaviour of several other polymers in different solvents. The influence of polymer type and solvent on measured τ values will be compared to predictions from the DiMarzio–Guttman model, the model that appeared to match closely the minimum τ values for PS in THF.

HDC of polymers in a good solvent

For all polymer types used (PS, PB, PIP and PMMA), THF appears to be a good solvent. In this solvent we can expect that the polymer chains are more swollen than in their unperturbed state. Because of differences in unperturbed dimensions and expansion factors, the actual polymer size for a given molecular mass is greatly dependent on polymer type. For a given molecular mass, the coil size decreases (or compactness increases) in the order PB, PIP, PS, PMMA. The difference in mass density between different polymer types finds expression in different r_G–M_w relationships. This can be seen from the relationships, summarized in Table III. For PS an r_G–M_w relationship is known from light-scattering measurements. For the other polymers, r_G–M_w relationships were obtained from eqn. 3, using the measured Mark–Houwink constants.

Applying the r_G–M_w relationships from Table III, theoretical calibration graphs according to eqn. 11, using C_{DG} and $r_p = r_{eff}$, are constructed in Fig. 8. As M_w instead of polymer size is plotted against τ, the curves for the different polymers do not overlap. Obviously, for the more tightly coiled polymer types, the calibration graph is shifted towards higher molecular mass. The good match between the theoretical curve and the experimental data, found earlier for PS, appears to hold also for other polymer types. The difference in compactness between the polymer types appears to influence migration only through its effect on coil size.

It may be argued that the difference in segment density may also influence migration through its impact on the permeability of the chain. We have already discussed that the solvent in the core of the chain is almost fully immobil-

TABLE III

RELATIONSHIPS BETWEEN r_G AND M_w FOR POLYMERS IN THF

Polymer	r_G–M_w relationship
PB	Eqn. 3; $K = 5.023 \cdot 10^{-2}$ (ml/g) and $a = 0.683$
PIP	Eqn. 3; $K = 1.25 \cdot 10^{-2}$ (ml/g) and $a = 0.775$
PS	$r_G = 1.39 \cdot 10^{-5} M_w^{0.588}$ (μm)[a]
PMMA	Eqn. 3; $K = 0.7998 \cdot 10^{-2}$ (ml/g) and $a = 0.734$

[a] Ref. 5.

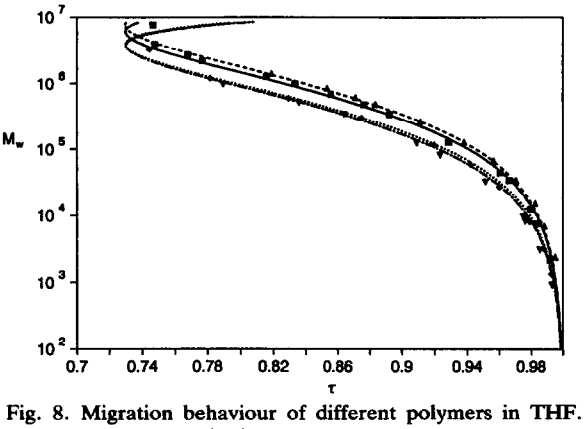

Fig. 8. Migration behaviour of different polymers in THF. Column as in Fig. 4; $\langle v_m \rangle = 0.22$ mm/s. The theoretical lines are drawn according to the modified DiMarzio–Guttman model with $r_p = r_{eff}$ and $C_{DG} = 2.698$. The experimental points and theoretical lines are for (▲, - - - -) PMMA, (■, ————) PS, (◆, ·····) PIP and (▼, -·-·-·-·-) PB.

ized with respect to the coil, but also that the flow permeability increases on going from the interior towards the outside of the chain. In the chain domains with partial draining, the segment density may be an important factor influencing the flow permeability. Increasing the segment density of a linear polymer coil is expected to increase the degree of solvent immobilization. In other words, the segment density of the coil affects the distance from the mass centre at which the solvent is effectively immobilized with respect to the chain. As this distance is proportional to r_h, it may be expected that the ratio r_h/r_G is dependent on the compactness of the polymer chain and thus on the type of polymer. This was indeed found experimentally, using different types of linear polymers, although the differences measured were very small. In both good and poor solvents, the ratio r_h/r_G was reported to increase slightly in the order PB, PIP, PS [41]. In our modification of the Brenner–Gaydos model (eqn. 14), a change in the r_h/r_G ratio alters C_{BG}. According to the experimental results, there is no indication that the C value should vary notably among the different polymer types.

When the calibration graphs are plotted with polymer size or λ as the abscissa and τ as the ordinate, the lines for the different polymer types in Fig. 8 will coincide. This means that a universal calibration graph is valid, just as in SEC [61]. Such a graph, drawn in Fig. 9, indeed shows that all experimental points fall on one line, which can be described accurately by the DiMarzio–Guttman model.

As the migration rate of polymers is determined by their size, it is possible to separate polymers with different segment density but equal molecular mass. In Fig. 10, this is demonstrated for a PB, PIP and PS fraction of about equal molecular mass. As predicted by theory, the polymer fractions elute in order of decreasing size.

Effect of solvent goodness on polymer migration in HDC

In the good solvent THF, the migration rate was found to be predicted well by the modified DiMarzio–Guttman model. In this section it will

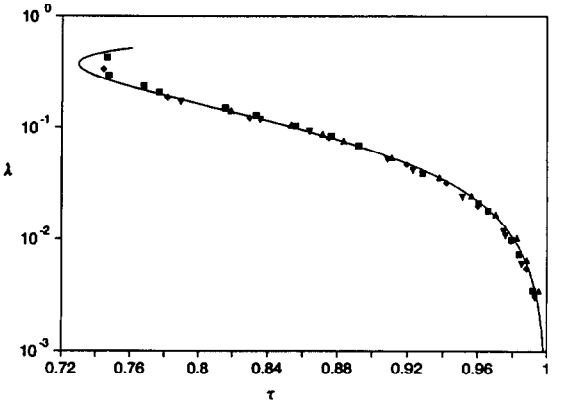

Fig. 9. Universal calibration graph for HDC. Experimental points as in Fig. 8. The theoretical line is drawn according to the modified DiMarzio–Guttman model with $r_p = r_{eff}$ and $C_{DG} = 2.698$.

be investigated whether this still holds when solvent conditions and hence the size of the coil are changed. Both good and poor solvents were used to study the effect of solvent power on the migration rate of polymers. In order to prevent adsorption of the polymers on the silica packing materials, only fairly polar solvents were regarded as suitable.

As poor solvents we selected θ-solvents

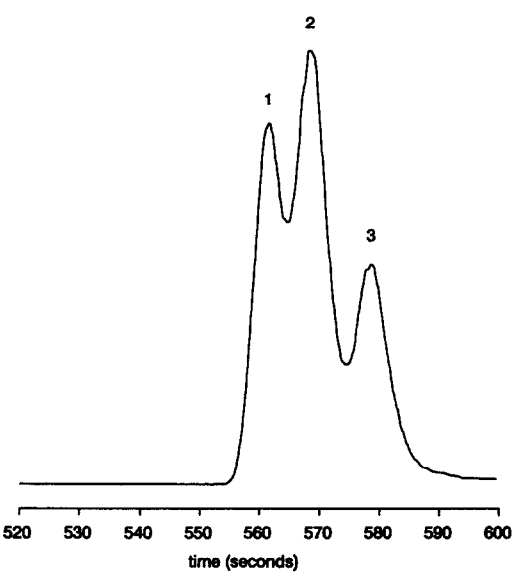

Fig. 10. Separation of different polymers of about equal molecular mass. Column as in Fig. 4; pressure drop, 28 bar; detection, ELSD. Solutes: (1) PB 330 000, (2) PIP 295 000 and (3) PS 336 000 in THF (0.10–0.15 mg/ml each).

because in that case reliable r_G–M_w relationships are known. For proper column thermostating, solvents were chosen with θ-temperatures between 20 and 45°C. The solvents used with their θ-temperatures and r_G–M_w relationships are summarized in Table IV. For PB and PIP, the literature data presented are those for polymer samples that match as closely as possible the isomer composition of our samples. For PS, a mixed solvent was used because candidate pure solvents were not suitable in the detectors used. The r_G–M_w relationships show that for the different polymers, the order of increasing compactness in a θ-solvent is the same as in THF.

Polybutadienes. When we switch from THF to a θ-solvent we may expect a substantial decrease in polymer size. This is indeed reflected in the observed migration behaviour, as shown in Fig. 11. The calibration graph for PB dissolved in dioxane at the θ-temperature is shifted towards smaller polymer sizes compared with the THF data. The theoretical calibration graph for the θ-solvent with $r_p = r_{eff}$ is in fairly good agreement with the experimental points, but the fit is not as good as for the good solvent THF. A better fit is obtained when r_G is taken as the polymer radius. As there is no physical reason to take r_G instead of r_{eff}, it is tempting to address this effect to a shortcoming of the capillary migration models in terms of their inability to describe properly flow in a packed column.

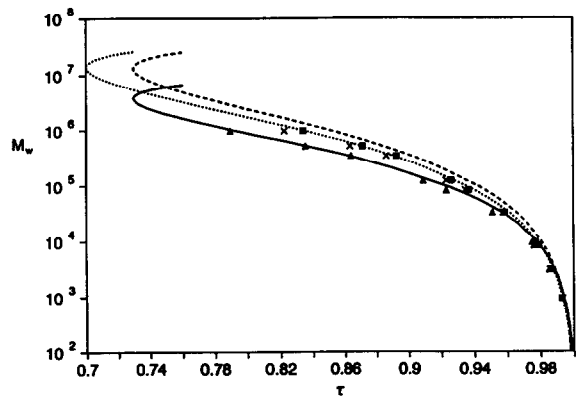

Fig. 11. Migration behaviour of PB in good and poor solvents. Column as in Fig. 4; $\langle v_m \rangle = 0.22$ mm/s. Experimental points: (▲) PB in THF, (■) PB in dioxane at 26.5°C and (×) PB in dioxane at 40.0°C. Theoretical lines are according to the modified DiMarzio–Guttman model. The lines are for PB in THF using $r_p = r_{eff}$ (———), PB in a θ-solvent using $r_p = r_{eff}$ (– – – –) and PB in a θ-solvent using $r_p = r_G$ (·····).

However, the same effect was also observed in capillary HDC of PS [5]. A possible explanation might be connected with the segment density distribution in a coil, which changes substantially when solvent conditions are changed [32].

Near the θ-point, the polymer size depends strongly on temperature. This is in contrast to good solvents where the polymer size hardly varies in a large temperature range. For PB in dioxane, we find that a temperature increment of

TABLE IV

θ CONDITIONS AND r_G–M_w RELATIONSHIPS FOR DIFFERENT POLYMERS

Polymer	Isomer composition	θ-Solvent	r_G–M_w relationship	Ref.
PB	*cis*:*trans* = 55:45–59:41; 8–11% 1,2-	Dioxane; 26.5°C	$r_G = 3.79 \cdot 10^{-5} M_w^{0.50}$ (μm)	62
PIP	70% *cis*, 23% *trans*, 7% 3,4-	Dioxane; 34.7°C	$r_G = 3.35 \cdot 10^{-5} M_w^{0.50}$ (μm)	63
	84% *cis*, 14% *trans*, 2% 1,2-	Dioxane; 34°C		34
PS		Dioxane–methanol (65.1:34.9, v/v); 34.0°C	$r_G = 2.74 \cdot 10^{-5} M_w^{0.50}$ (μm)	34
PMMA		Acetonitrile; 44.0°C	$r_G = 2.56 \cdot 10^{-5} M_w^{0.50}$ (μm)[a]	64

[a] Evaluated from data in ref. 64 for $M_w > 10^4$.

13°C above the θ-temperature yields significantly lower τ values. This is in qualitative agreement with the expected size increment. In THF a similar temperature rise resulted in a decrease in τ of less than 0.001.

Polyisoprenes. The migration behaviour of PIP in a good and a poor solvent is shown in Fig. 12. In the poor solvent dioxane, the largest PIP of molecular mass 3 300 000 could not be detected because of too low solubility. The effect of solvent on the migration behaviour of PIP is almost exactly the same as found for PB. In a θ-solvent we arrive at much higher τ values than in THF. Again we find that for a good solvent the data agree well with the graph based on r_{eff} whereas for the poor solvent r_G is a better size parameter. The strong influence of temperature on polymer size in a θ-solvent is once more demonstrated by the strong temperature dependence of τ in dioxane.

Polystyrenes. Thermodynamically, butanone is a poorer solvent for PS than THF. Consequently, the polystyrenes are smaller in butanone than in THF. From Fig. 13, it appears that this is in agreement with the experimentally observed shift in τ values when using butanone instead of THF. For the highest molecular masses, however, an unexpected reversal was found in the

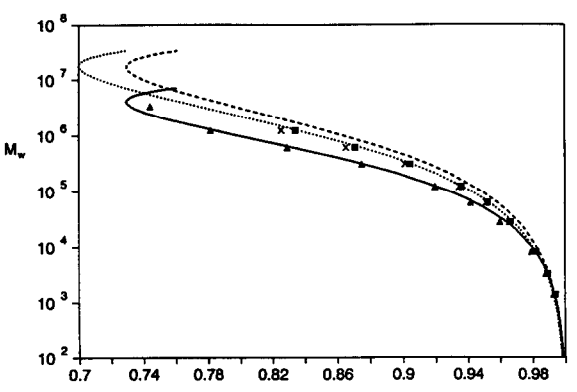

Fig. 12. Migration behaviour of PIP in good and poor solvents. Column as in Fig. 4; $\langle v_m \rangle = 0.22$ mm/s. Experimental points: (▲) PIP in THF, (■) PIP in dioxane at 34.0°C and (×) PIP in dioxane at 40.0°C. Theoretical lines are according to the modified DiMarzio–Guttman model. The lines are for PIP in THF using $r_p = r_{eff}$ (————), PIP in a θ-solvent using $r_p = r_{eff}$ (– – – –) and PIP in a θ-solvent using $r_p = r_G$ (·····).

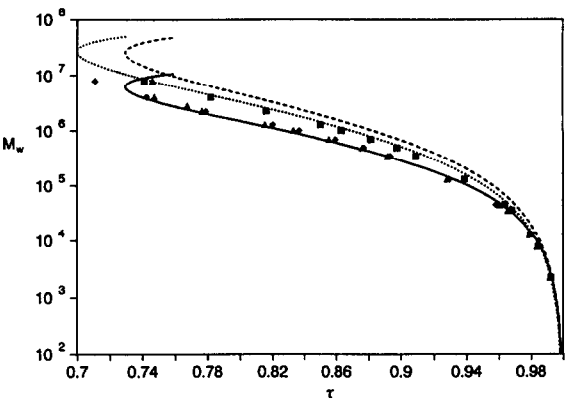

Fig. 13. Migration behaviour of PS in good and poor solvents. Column as in Fig. 4; $\langle v_m \rangle = 0.22$ mm/s. Experimental points: (▲) PS in THF, (◆) PS in butanone and (■) PS in dioxane –methanol at 34.0°C. Theoretical lines are according to the modified DiMarzio–Guttman model. The lines are for PS in THF using $r_p = r_{eff}$ (————), PS in a θ-solvent using $r_p = r_{eff}$ (– – – –) and PS in a θ-solvent using $r_p = r_G$ (·····).

elution order. Further decreasing the coil dimensions by switching to a θ-solvent gives larger τ values, as expected. Similar to the results for PB and PIP, the data for the θ-solvent are best fitted when $r_p = r_G$ is substituted in the DiMarzio–Guttman model, whereas in THF, r_{eff} appears to be a more suitable size measure.

Poly(methyl methacrylate)s. Also for the most compact polymer PMMA, the migration behaviour in acetonitrile at the θ-temperature is fitted best by the DiMarzio–Guttman model, provided $r_p = r_G$ is chosen in Fig. 14. The fit at low molecular masses is not very accurate, for unknown reasons. The deviations from the theoretical line are too large to be explained by the different r_G–M_w dependence that is usually found for lower molecular masses.

CONCLUSIONS

Columns packed with 1.5-μm non-porous particles are able to provide high-resolution separations for polymers having molecular masses between roughly 10^4 and $5 \cdot 10^6$. Despite the limited volume range available for peak elution, high resolution and a high peak capacity are possible owing to the very small dispersion. The dispersion being virtually independent of eluent

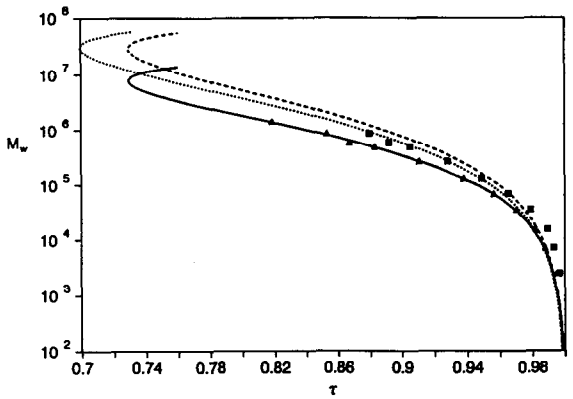

Fig. 14. Migration behaviour of PMMA in good and poor solvents. Column as in Fig. 4; $\langle v_m \rangle = 0.22$ mm/s. Experimental points: (▲) PMMA in THF and (■) PMMA in acetonitrile at 44.0°C. Theoretical lines are according to the modified DiMarzio–Guttman model. The lines are for PMMA in THF using $r_p = r_{eff}$ (————), PMMA in a θ-solvent using $r_p = r_{eff}$ (– – – –) and PMMA in a θ-solvent using $r_p = r_G$ (·····).

velocity allows for high-resolution separations in a short analysis time.

The migration behaviour for polymers of high molecular mass appears to depend slightly on eluent velocity. This phenomenon has not yet been included in the simple migration models which have been applied to packed columns so far. In a limited (but for practical use nevertheless very important) range of eluent velocities, the migration behaviour for linear random coil polymers in THF is observed to be accurately represented by the modified DiMarzio–Guttman model for open tubes. In this model the effective polymer radius is taken as the radius determining exclusion. The DiMarzio–Guttman model being successful for different types of linear polymers indicates that, at fixed eluent velocity, the migration depends on the size of the coil but not on its segment density. For this reason, a universal calibration graph was found to hold in HDC, as in SEC. Also for a very poor solvent (a θ-solvent), the DiMarzio–Guttman model was in good agreement with experimental data. However, to obtain such agreement it was necessary to take the radius of gyration as the radius determining exclusion. This has been reported before in capillary HDC. It was further shown that HDC is a suitable method for monitoring small changes in coil dimensions when, for instance, the nature of the solvent is varied.

SYMBOLS

a	Mark–Houwink constant
C	slip factor
D_m	molecular diffusion coefficient (m^2/s)
De	Deborah number
d_p	particle diameter (m)
$E(r)$	dimensionless potential working on a particle
K	Mark–Houwink constant (ml/g)
L	column length (m)
l	segment length (m)
M	molecular mass (g/mol)
M_n	number-average relative molecular mass
M_w	mass-average relative molecular mass
n	number of segment units in a chain
ΔP	pressure drop across the column (N/m^2)
Pe	Péclet number, $2\langle v_m \rangle R/D_m$
R	radius of a tube (m)
R_0	hydraulic radius of a packed column, $d_p\epsilon/3(1-\epsilon)$ (m)
Re	Reynolds number
r	radial position
r_{eff}	effective radius of a polymer chain, $0.886r_G$ (m)
r_G	radius of gyration (m)
$\langle r_G^2 \rangle$	mean square radius of gyration (m^2)
$\langle r_G^2 \rangle_0$	mean square radius of gyration of an unperturbed chain (m^2)
r_h	hydrodynamic radius (m)
r_p	particle or polymer radius determining wall exclusion (m)
r_s	radius of a (equivalent) solid sphere (m)
V_c	total column volume (m^3)
V_0	interparticle volume (m^3)
$\langle v_m \rangle$	average mobile phase velocity (m/s)
$\langle v_p \rangle$	average polymer or particle velocity (m/s)
$v_p(r)$	local axial particle velocity (m/s)
$v_s(r)$	local particle slip velocity (m/s)
α	linear expansion factor
β	solvent strength parameter
γ	wall-effect parameter
ϵ	column porosity
η	dynamic viscosity (Ns/m^2)

λ	aspect ratio, r_p/R
σ	structural parameter
τ	dimensionless migration rate, $\langle v_m \rangle / \langle v_p \rangle$
ϕ_0	Flory universal constant (mol^{-1})
φ	column resistance parameter

ACKNOWLEDGEMENTS

The authors thank Dr. F.A. Buytenhuys and H.J.F.M. van de Ven (Akzo Research Laboratories, Arnhem, Netherlands) for determining Mark–Houwink constants. This research was supported by the Netherlands Foundation for Chemical Research (SON), with financial aid from the Netherlands Organization for Scientific Research (NWO) under grant 700-344-003.

REFERENCES

1 A.J. McHugh, *CRC Crit. Rev. Anal. Chem.*, 15 (1984) 63.
2 A.W.J. Brough, D.E. Hillman and R.P. Perry, *J. Chromatogr.*, 208 (1981) 175.
3 H. Small, *J. Colloid Interface Sci.*, 48 (1974) 147.
4 J.C. Kraak, R. Oostervink, H. Poppe, U. Esser and K.K. Unger, *Chromatographia*, 27 (1989) 585.
5 R. Tijssen, J. Bos and M.E. van Kreveld, *Anal. Chem.*, 58 (1986) 3036.
6 D.A. Hoagland and R.K. Prud'homme, *J. Appl. Polym. Sci.*, 36 (1988) 935.
7 R.K. Prud'homme, G. Froiman and D.A. Hoagland, *Carbohydr. Res.*, 106 (1982) 225.
8 D.A. Hoagland and R.K. Prud'homme, *Macromolecules*, 22 (1989) 775.
9 R.J. Noel, K. Gooding, F.E. Regnier, D.M. Ball, C. Orr and H.E. Mullins, *J. Chromatogr.*, 166 (1978) 373.
10 P. Elie and M. Renaud, *Entropie*, 136 (1987) 33.
11 P. Elie and M. Renaud, *Entropie*, 115 (1984) 27.
12 G. Stegeman, R. Oostervink, J.C. Kraak, H. Poppe and K.K. Unger, *J. Chromatogr.*, 506 (1990) 547.
13 K.O. Pedersen, *Arch. Biochem. Biophys., Suppl.*, 1 (1962) 157.
14 D.A. Hoagland, K.A. Larson, R.K. Prud'homme, *Polym. Mater. Sci. Eng.*, 51 (1984) 543.
15 F.J. Molina, A.O. Vila, P. Dieguez, J.E. Figueruelo, *J. High Resolut. Chromatogr.*, 12 (1989) 560.
16 E.A. DiMarzio and C.M. Guttman, *J. Polym. Sci., Part B*, 7 (1969) 267.
17 E.A. DiMarzio and C.M. Guttman, *Macromolecules*, 3 (1970) 131 and 681.
18 E.A. DiMarzio and C.M. Guttman, *J. Chromatogr.*, 55 (1971) 83.
19 H. Brenner and L.J. Gaydos, *J. Colloid Interface Sci.*, 58 (1977) 312.
20 H. Small, F.L. Saunders and J. Solc, *Adv. Colloid Interface Sci.*, 6 (1976) 237.
21 D.C. Prieve and P.M. Hoysan, *J. Colloid Interface Sci.*, 64 (1978) 201.
22 C.A. Silebi and A.J. McHugh, *AIChE J.*, 24 (1978) 204.
23 B.A. Buffham, *J. Colloid Interface Sci.*, 67 (1978) 154.
24 C.A. Silebi and J.G. DosRamos, *J. Colloid Interface Sci.*, 130 (1989) 14.
25 G. Segré and A. Silberberg, *J. Fluid Mech.*, 14 (1962) 136.
26 J.G. DosRamos and C.A. Silebi, *J. Colloid Interface Sci.*, 133 (1989) 302.
27 H.J. Ploehn, *Int. J. Multiphase Flow*, 13 (1987) 773.
28 J. Lecourtier and G. Chauveteau, *Macromolecules*, 17 (1984) 1340.
29 M.A. Langhorst, F.W. Stanley, Jr., S.S. Cutié, J.H. Sugarman, L.R. Wilson, D.A. Hoagland, R.K. Prud'homme, *Anal. Chem.*, 58 (1986) 2242.
30 R. Tijssen and J. Bos, in F. Dondi and G. Guiochon (Editors), *Theoretical Advancement in Chromatography and Related Separation Techniques*, Kluwer, Dordrecht, 1992, pp. 397–441.
31 P.J. Flory, *Principles of Polymer Chemistry*, Cornell University Press, Ithaca, NY, 1971.
32 H. Yamakawa, *Modern Theory of Polymer Solutions*, Harper & Row, New York, 1971.
33 A. Dondos and H. Benoit, *Macromolecules*, 4 (1971) 279.
34 J. Brandrup and E.H. Immergut (Editors), *Polymer Handbook*, Wiley Interscience, New York, 3rd ed., 1989.
35 O.B. Ptitsyn and Y.E. Eizner, *Sov. Phys. Tech. Phys.*, 4 (1960) 1020.
36 W.W. Yau, J.J. Kirkland and D.D. Bly, *Modern Size Exclusion Liquid Chromatography*, Wiley, New York, 1979.
37 M.E. van Kreveld and N. van den Hoed, *J. Chromatogr.*, 83 (1973) 111.
38 J. Roovers and J.E. Martin, *J. Polym. Sci., Part B*, 27 (1989) 2513.
39 J.J.H. Mulderije and H.L. Jalink, *Macromolecules*, 20 (1987) 1152.
40 H. Brenner, *Adv. Chem. Eng.*, 6 (1966) 287.
41 A.J. Goldman, R.G. Cox and H. Brenner, *Chem. Eng. Sci.*, 22 (1967) 653.
42 S. Bantle, M. Schmidt and W. Burchard, *Macromolecules*, 15 (1982) 1604.
43 L.G. Leal, *Annu. Rev. Fluid Mech.*, 12 (1980) 435.
44 Y. Cohen, in N.P. Cheremisinoff (Editor), *Encyclopedia of Fluid Mechanics, Vol, 7, Rheology and Non-Newtonian Flows*, Gulf, Houston, TX, 1988, Ch. 14.
45 M. Tirell and M.F. Malone, *J. Polym. Sci., Polym. Phys. Ed.*, 15 (1977) 1569.
46 A.B. Metzner, Y. Cohen and C. Rangel-Nafaile, *Non-Newtonian Fluid Mech.*, 5 (1979) 449.
47 Y. Cohen and A.B. Metzner, *Chem. Eng. Commun.*, 41 (1986) 73.
48 M. Tirrell and M.F. Malone, *J. Polym. Sci., Polym. Phys. Ed.*, 15 (1977) 1569.

49 G. Stegeman, J.C. Kraak and H. Poppe, *J. Chromatogr.*, 550 (1991) 721.
50 J.H. Aubert and M. Tirrell, *J. Chem. Phys.*, 72 (1980) 2694.
51 J.H. Aubert and M. Tirrell, *Rheol. Acta*, 19 (1980) 452.
52 G. Sekhon, R.C. Armstrong and M.S. Ihon, *J. Polym. Sci., Polym. Phys. Ed.*, 20 (1982) 947.
53 P.O. Brunn, *Int. J. Multiphase Flow*, 9 (1983) 187.
54 P.O. Brunn and S. Chi, *Rheol. Acta*, 23 (1984) 163.
55 R.H. Shafer, M. Laiken and B.H. Zimm, *Biophys. Chem.*, 2 (1974) 180.
56 J.H. Aubert and M. Tirrell, *J. Liq. Chromatogr.*, 6 (1983) 219.
57 J.C. Giddings, *Sep. Sci. Technol.*, 13 (1978) 241.
58 G. Stegeman, J.C. Kraak, H. Poppe, *J. Chromatogr.*, 634 (1993) 149.
59 J.C. Giddings, *Adv. Chromatogr.*, 20 (1982) 217.
60 J.C. Giddings, M. Martin and M.N. Meyers, *J. Chromatogr.*, 158 (1978) 419.
61 H. Benoit, Z. Grubisic, P. Rempp, D. Dekker and J.G. Zilliox, *J. Chim. Phys.*, 63 (1966) 1507.
62 J. Roovers, P. Toporowski and J. Martin, *Macromolecules*, 22 (1989) 1897.
63 Y. Tsunashima, M. Hirata, N. Nemoto, K. Kajiwara and M. Kurata, *Macromolecules*, 20 (1987) 2862.
64 Y. Tamai, T. Konishi, Y. Einaga, M. Fujii and H. Yamakawa, *Macromolecules*, 23 (1990) 4075.